THE RHEOLOGY AND ERUPTION CONDITIONS OF FISSURE-FED LAVAS NEAR JOVIS THOLUS, MARS. Marissa Lo[1,2], Lionel Wilson[2] and Magdalena Oryaëlle Chevrel[3], [1]School of Earth and Environmental Sciences, University of Manchester, Manchester M13 9PL, UK (marissa.lo@postgrad.manchester.ac.uk), [2]Lancaster Environment Centre, Lancaster University, Lancaster LA1 4YQ, UK, [3]Laboratoire Magmas et Volcans, Université Clermont Auverge, 63178 Aubière, France (o.chevrel@opgc.fr).

Introduction: The morphology of lava flows on Mars has been used to infer the rheological properties and composition of the erupting lava, e.g. [1-15]. The availability of data on the rheological properties of lavas whose compositions can be used as proxies for lava compositions on Mars [16-17] has prompted us to revisit the flows from a fissure system to the east of the volcano Jovis Tholus in the Tharsis region of Mars (~18.3 °N,~245.5 °E - Fig. 1) first studied by [13]. We aim to constrain the combinations of lava rheology and eruption conditions that gave rise to the observed flows.

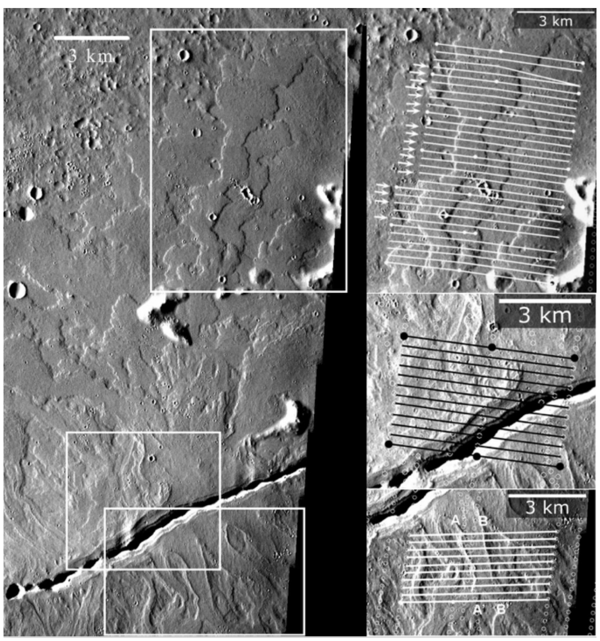

Fig. 1. An undrained flow, a fissure with ramparts, and a drained flow with prominent levees in the Tharsis region, Mars, previously studied by [13].

Study area: Fig. 1, left side, shows the 3 features analyzed: a largely undrained lava flow (top), the spatter ramparts along the north side of the fissure (middle) and a drained flow with prominent residual levees (bottom). The panes on the right show the approximately east-west photoclinometric topographic profiles produced by [13] and the MOLA elevation data points (black or white spots) to which they are anchored.

Methods and Results: For each topographic profile, the underlying topography was interpolated. The deposit thickness d and the slope, α, of the ground under the deposit were recorded. Given the geometry, only the approximately east-west and north-south slopes were measureable, and the larger of the two was adopted. The density of the lava, ρ, was taken as 2500 kg m^{-3}. It was assumed that all of the ramparts and levees, and the undrained flow, had reached their final configuration as a result of the shear stress at the base just being equal to the lava yield strength y, which was evaluated for each measured point from $y = \rho\, g\, d \sin \alpha$ where g is the acceleration due to gravity, 3.72 m s^{-2}. Yield strength values are shown in Table 1 as a function of distance, x, from the vent for the flows, and of distance along strike for the spatter rampart of the fissure .

Table 1. Yield strength measurements.

Undrained flow

x/km	d/m	α/deg.	y/Pa
13.4	2.8	0.23	105
13.7	3.8	0.23	142
14.0	3.7	0.15	92
14.6	3.0	0.19	94
14.9	3.0	0.19	94
15.2	3.1	0.61	309
15.5	2.5	0.06	23
15.8	2.2	0.61	220
16.1	2.8	0.01	4
16.4	2.6	0.26	109
16.7	2.3	0.12	43
17.0	2.7	0.42	185
17.3	3.2	0.27	140
17.6	2.8	0.33	148
17.9	2.0	0.21	69
18.2	4.5	0.10	70
18.5	3.8	0.12	71
18.8	3.3	0.07	36

Spatter Rampart

no.*	d/m	α/deg.	y/kPa
1	4.8	18.4	14
2	6.7	17.6	19
3	7.9	20.1	25
4	6.1	13.6	13
5	5.2	2.1	2
6	7.1	15.2	17
7	6.5	3.1	3
8	8.4	10.5	14
9	8.4	7.9	11
10	5.9	6.9	7
11	7.5	24.6	29
12	5.3	5.8	5

Drained Flow

x/km	d/m	α/deg.	y/Pa
3.0	1.7	0.342	94
3.3	2.4	0.342	130
3.6	2.1	0.342	116
3.9	1.6	0.342	88
4.2	1.7	0.342	94
4.5	1.5	0.342	83
4.8	2.0	0.342	110

*Profiles are numbered 1 to 12, North to South.

Discussion: Numerous results follow from Table 1:

(a) The yield strength values show great scatter, almost certainly due to the difficulty of accurately estimating the pre-eruption topography and hence the deposit thickness, but they do not exhibit significant trends with distance from the vent or position along the fissure.

(b) The yield strength of the fissure rampart material, 13 kPa, is more than 100 times greater than that of the flows. The spatter rampart material is stratigraphically younger than the flow material and so erupted toward the end of the eruption. We infer that this material accumulated from fire fountains in which pyroclasts lost heat efficiently, in contrast to the flows, which were fed by fountains containing clasts that lost little heat. The heat-retention properties of fire fountains are a function of mean pyroclast size and number density [18]. Number density is in turn dependent on released magma gas content, which drives the height of the fountain, and magma volume flux, which determines the rate at which new clasts enter the fountain. The simplest explanation of the implied pyroclast temperature trend is that the rise speed, and hence erupted volume flux, of magma decreased significantly toward the end of the eruption.

(c) The yield strengths of both flows are essentially identical, averaging 109 Pa for the undrained flow and 102 Pa for the drained flow. The fact that there is no significant increase in yield strength with distance from the vent is consistent with the behaviour of laminar flows, where a near-isothermal core is insulated by slowly growing thermal boundary layers. This contrasts with the behaviour of turbulent flows, where extreme stirring cools the entire bulk of the flow causing a rapid increase in crystal content and yield strength. There is therefore no obvious evidence of turbulent flow having been involved in this eruption.

(d) Chevrel et al. [16, their Fig. 6] have summarized observational and theoretical models of how yield strength, y, varies with crystal content for Mars-like magmas. Considering crystals with high aspect ratios, we find that yield strengths in the range 102-109 Pa correspond to 25-33 vol.% crystallization.

(e) Chevrel et al. [17, their Figs. 10 and 11] provide data linking crystallinity, temperature, T, and viscosity, η, for Mars-like magmas. The above range of crystal contents would correspond to temperatures of 1425-1415 K, which in terms of viscosity (applying the fitting parameters of [19] for needle-like crystals) would correspond to viscosities of ~10^2 - 10^4 Pa s. This wide range of viscosity values is due to the high level of disagreement between the various yield strength-crystal content models summarized by [16]. Given that the final configuration of lava flow deposits records conditions as the flow is coming to rest, we take the lower end of the viscosity range to be relevant and adopt $\eta = 100$ Pa s.

(f) With this viscosity estimate we can now use the width, w, thickness, d, and substrate slope, α, at each measured point along the undrained flow to find the flow speed, u, and hence the volume flux, $V = w\,d\,u$. We evaluated the speed using the standard formulae for both laminar and turbulent flow and checked which was appropriate by evaluating the implied Reynolds numbers. In all cases the flow motion was found to be laminar. Table 2 contains the results.

Table 2. Flow dynamics.

x /km	w /m	d /m	α /deg.	u /(m/s)	V /(m³/s)
13.4	2303	2.8	0.23	0.85	5483
13.7	4816	3.8	0.23	1.57	28658
14.0	3827	3.7	0.15	0.99	14018
14.6	2731	3.0	0.19	0.81	6664
14.9	2951	3.0	0.19	0.81	7201
15.2	2416	3.1	0.61	2.78	20812
15.5	1959	2.5	0.06	0.17	830
15.8	1778	2.2	0.61	1.40	5474
16.1	1880	2.8	0.01	0.04	186
16.4	1548	2.6	0.26	0.82	3319
16.7	2008	2.3	0.12	0.29	1324
17.0	2975	2.7	0.42	1.45	11642
17.3	4078	3.2	0.27	1.30	16905
17.6	3228	2.8	0.33	1.20	10885
17.9	2423	2.0	0.21	0.40	1927
18.2	5936	4.5	0.10	0.91	24431
18.5	5144	3.8	0.12	0.78	15298
18.8	4294	3.3	0.07	0.34	4879

Results: Again, there is inevitably great scatter in the volume flux, but there is no systematic trend, and the mean value is 10,000 $m^3\ s^{-1}$ (with a formal standard deviation of ± 8500 $m^3\ s^{-1}$). The measured part of the ~20 km long undrained flow unit has a mean width of 3130 m and a mean thickness of 3.0 m, implying a volume of 0.19 km^3, and so the implied emplacement time is 19,000 s or ~5.3 hours, with a mean speed very close to 1 $m\ s^{-1}$.

References: [1] Hulme G. (1976) *Icarus, 27*, 207–213. [2] Zimbelman J. R. (1985) *JGR, 90,* 157-162. [3] Zimbelman J. R. (1998) *JGR, 103*, 27,503–27,516. [4] Baloga S. M. et al. (2003) *JGR*, *108*, 1–10. [5] Glaze L. S. et al. (2003). *Icarus*, *165*, 26–33. [6] Rowland S. K. et al. (2004) *JGR*, *109,* E10010**,** 16. pp [7] Glaze L. S. and Baloga S. M. (2006). *JGR*, *111*, E09006, 10 pp. [8] Garry W. B. et al. (2007) *JGR, 112*, E08007, 21 pp. [9] Hiesinger H. et al. (2007) *JGR*, *112,* E05011, 24 pp. [10] Baloga S. M. and Glaze L. S. (2008) *JGR*, *113* E05003, 15 pp. [11] Glaze L. S. et al. (2009) *JGR - Planets, 114*, E07001, 15 pp. [12] Vaucher J. et al. (2009) *Icarus*, *200*, 39–51. [13] Wilson L. et al. (2009) *JVGR*, *185*, 28–46. [14] Jaeger W. L. et al. (2010) *Icarus*, 205, 230–243. [15] Pasckert J. H. et al. (2012) *Icarus*, *219*, 443–457. [16] Chevrel M. O. et al. (2013) *EPSL*, *384*, 109–120. [17] Chevrel M. O. et al. (2014) *GCA*, *124*, 348–365. [18] Wilson L. and Head J. W. (2017) *Icarus*, *283*, 146–175. [19] Cimarelli C. et al. (2011) *Geochem. Geophys. Geosys., 12*, Q07024.